



A W-band Quasi-Optical Array Antenna Feeding Network with High Taper Efficiency Using Optimal Ridge Excitation of an H-Plane Sectoral

Downloaded from: <https://research.chalmers.se>, 2024-06-29 20:35 UTC

Citation for the original published paper (version of record):

Zhang, Y., Vilenskiy, A., Litun, V. et al (2024). A W-band Quasi-Optical Array Antenna Feeding Network with High Taper Efficiency Using Optimal Ridge Excitation of an H-Plane Sectoral Waveguide. *IEEE Antennas and Wireless Propagation Letters*. <http://dx.doi.org/10.1109/LAWP.2024.3404351>

N.B. When citing this work, cite the original published paper.

© 2024 IEEE. Personal use of this material is permitted. Permission from IEEE must be obtained for all other uses, in any current or future media, including reprinting/republishing this material for advertising or promotional purposes, or reuse of any copyrighted component of this work in other works.

This document was downloaded from <http://research.chalmers.se>, where it is available in accordance with the IEEE PSPB Operations Manual, amended 19 Nov. 2010, Sec. 8.1.9. (<http://www.ieee.org/documents/opsmanual.pdf>).

(article starts on next page)

A W-band Quasi-Optical Array Antenna Feeding Network with High Taper Efficiency Using Optimal Ridge Excitation of an H-Plane Sectoral Waveguide

Yingqi Zhang, *Student Member, IEEE*, Artem R. Vilenskiy, *Member, IEEE*, Vladimir I. Litun, *Senior Member, IEEE*, and Marianna V. Ivashina, *Senior Member, IEEE*

Abstract—A novel H-plane quasi-optical (QO) feeding network for linear (sub-)array gap waveguide (GWG) antennas intended for beam-steering applications at W-band is presented. The QO feed comprises an H-plane sectoral GWG excited by an input stepped ridge gap waveguide (RGW) and transitioned to an overmoded rectangular groove gap waveguide (GGW) section, the latter being terminated with an array of RGW output probes. This work's key challenge and novelty is engineering the desired modal content in the QO structure for uniform amplitude excitation of array elements to enhance antenna gain with a low insertion loss. This was addressed by (i) realizing an optimal multi-mode excitation of the sectoral GWG and (ii) a proper phasing of a rich modal spectrum of the output overmoded GGW. An eigenmode-based semi-analytic approach was developed to investigate the impact of an input ridge length on the excited modal content and was shown to predict optimal results close to full-wave simulations. The demonstrated QO feed concept, applied to a 20-element array design, significantly outperforms existing solutions by achieving a 97% amplitude taper efficiency and showing less than 0.4 dB insertion loss over a 21% relative bandwidth (85–105 GHz).

Index Terms—quasi-optical feed, array antenna, gap waveguide.

I. INTRODUCTION

THE high-gain millimeter-wave antenna systems incorporating intelligent beamforming play an important role in advancing the next-generation 6G communication systems, in particular in the W-band (75-110 GHz) [1]. However, conventional phased-array antennas (PAAs) face challenges at these frequencies due to high material losses and constraints imposed by physically small element sizes and inter-element spacings. This, in turn, results in a substantial insertion loss in beamforming/feeding networks and difficulties in integrating front-end electronics [2], [3]. Recent studies have focused on improving PAA architectures by examining spatial or quasi-optical (QO) feeding networks, enabling efficient power transfer to antenna elements, which, combined with low-order

phase shifters (PSs), simplify a beamformer design [4]. These approaches are effective in sub-30 GHz frequencies [5], [6] and are being explored up to 100+ GHz [4], [7]. A 100 GHz linear array concept from [4], [8] contains an H-plane QO feeding network implemented in the gap waveguide (GWG) technology and low-order PSs that can be co-integrated with array elements to enable beam steering [9], [10].

A critical limitation of such QO feeding networks is the uneven (tapered) signal amplitude distribution at output ports, leading to a lower antenna gain [8], [11]–[17]. This issue stems from a field suppression in H-plane sidewall regions intrinsic for all waveguide (WG) structures. While addressing this problem with E-plane feeds is feasible [18], it comes at the cost of a significantly increased feed profile and limited types of applicable WGs. To date, most published 1-D H-plane QO feeding networks deal only with phase compensation mechanisms utilizing slow-wave structures [12]–[16], parabolic reflector [11], [19] and geodesic WG profiles [17]. As a result, they typically have a relatively high amplitude taper (≥ 15 dB) and low taper efficiency ($\leq 86\%$). Recently, Sabbaghi *et al.* [20] applied a linearly tapering (sectoral) ridge gap waveguide (RGW) that potentially can compensate for the edge tapering problem in H-plane horn antennas. However, this technique imposes a wideband impedance matching limitation for the case of 1-D PAAs [8].

Our work targets addressing this fundamental issue by achieving a nearly uniform output amplitude distribution of the H-plane QO feeding network, first presented in [8], through an optimal ridge excitation of the multi-modal H-plane sectoral GWG and its transition to an overmoded rectangular groove gap waveguide (GGW). Sections II and III describe the proposed idea and analysis methodology, while Section IV presents simulations, measurements, and comparisons with prior research. Conclusions are summarized in Section V.

II. GWG QO FEEDING NETWORK

The proposed design utilizes a bed of nails electromagnetic bandgap (EBG) surface, forming the contactless sidewalls of the GWG QO feeding network [4] (also referred to as QO feed), as shown in Fig. 1. The QO feed includes: (i) the input (reference) RGW protruding through the excitation area into (ii) the H-plane sectoral GWG, and (iii) overmoded rectangular GGW interfacing with the array of N_x output RGW probes. The properties of the EBG surface and reference RGW, as well as the configuration of the probes, have been described in [8].

Manuscript received xx xx, 2023; accepted xx xx, 2024. Date of publication XX XX, XXX. This work was carried out in the EUREKA EURIPIDES2 InnoStar project, Diarienummer 2021-0405, and supported in part by the Swedish Foundation for Strategic Research under Grant STP19-0043. (*Corresponding author: Y. Zhang*)

Y. Zhang, A. R. Vilenskiy, and M. V. Ivashina are with Antenna Systems Group, Dept. of Electrical Engineering, Chalmers University of Technology, 41296 Gothenburg, Sweden. (e-mail: yingqi@chalmers.se, artem.vilenskiy@chalmers.se, marianna.ivashina@chalmers.se).

V. I. Litun is with Ansys MEA FZ-LLC, Dubai, UAE (e-mail: vladimir.litun@ansys.com).

Digital Object Identifier XXXX

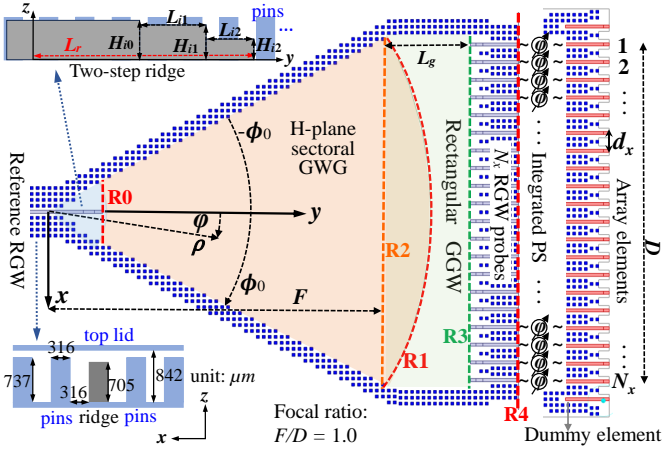


Fig. 1. A linear (sub-)array antenna with a QO beamforming network comprising a QO feed and integrated phase shifters in the GWG technology.

The spacing between the probes in the output array is denoted as $d_x = 0.6\lambda_0 = 1.896$ mm, where λ_0 is the free-space wavelength at the central design frequency $f_0 = 95$ GHz. The targeted design bandwidth (BW) is 85–105 GHz. The QO feed has a uniform height $H_0 = 842$ μm and the focal ratio $F/D = 1$ (the flare angle $2\phi_0 = 53^\circ$), which is optimal for PAAs with the low-order phase resolution [4], [8].

III. MODAL ANALYSIS OF THE QO FEED

A. Input RGW-to-Sectoral GWG Transition

Our first goal is to reach a maximum field amplitude uniformity on the reference plane R_1 (Fig. 1). This is achieved by exciting several propagating modes of the sectoral GWG, having specific complex coefficients. At the same time, the non-linear phase distribution of the sectoral GWG field is not compensated and is deliberately used for phase error randomization in the low-order phase resolution PAA [4]. In this study, we will approximate the EBG sidewalls by solid metal walls. This assumption was found valid for the WGs with a transverse size above a free-space wavelength λ .

For the given H_0 , only TM_{0p} (to z) modes can propagate in the sectoral WG region, having no variations along the z -axis [21]. Considering the structural symmetry, the total E-field of the sectoral GWG propagating along the positive y -direction can be written as a superposition of modal fields $\mathbf{e}_{0p}^{\text{sTM}}$:

$$\mathbf{E}^s(\rho, \phi) = \mathbf{z}^0 \sum_p A_{0p}^s \cos\left(\frac{p\pi\phi}{2\phi_0}\right) H_{p\pi/2\phi_0}^{(2)}(k\rho), \quad (1)$$

where A_{0p}^s are unknown modal complex coefficients; $H_{p\pi/2\phi_0}^{(2)}$ is the Hankel function of the second kind and order $p\pi/2\phi_0$; (ρ, ϕ) are the cylindrical coordinates; $k = 2\pi/\lambda$; $p = 1, 3, 5, \dots$. If we now assume an ideal uniform E-field distribution on the reference surface R_1 (Fig. 1), i.e. at $\rho_F = F/\cos(\phi_0)$, the desired optimal coefficients can be found analytically as $A_{0p}^{\text{sTM opt}}/A_{01}^{\text{sTM opt}} = (-1)^k/p$, $p = 2k + 1$, $k = 0, 1, 2, \dots$, where $A_{0p}^{\text{sTM}} = A_{0p}^s H_{p\pi/2\phi_0}^{(2)}(k\rho_F)$. E.g., $A_{03}^{\text{sTM opt}}$ should have a relative magnitude of around 0.33 and a 180° relative phase. Numerically, the sectoral GWG excitation problem can be formulated by enforcing the continuity of the tangential fields on the excitation reference plane R_0 :

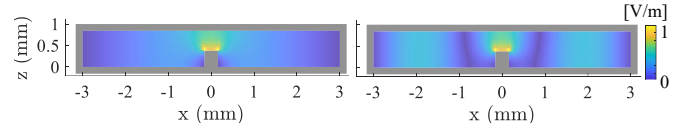


Fig. 2. Modal E-field magnitude distributions for the TE_{10} (left) and TE_{30} (right) modes of the ridge WG approximating the RGW on R_0 (95 GHz).

$$\mathbf{y}^0 \times \sum_{m,n} (A_{mn}^r \mathbf{e}_{mn}^{r+} + B_{mn}^r \mathbf{e}_{mn}^{r-}) = \mathbf{y}^0 \times \sum_{n,p} A_{np}^s \mathbf{e}_{np}^{s+}, \quad (2)$$

where $\mathbf{e}_{mn}^{r+/-}$ stand for forward and backward modal E-fields of the RGW interfacing R_0 , $A_{m,n}^r$ and $B_{m,n}^r$ are the corresponding modal coefficients; indices m and n define x - and z -variations, respectively. We note that the summations on both sides should in general include all TE and TM modes. Complemented by a similar equation for the H-field, (2) provides a full field equation system. Finally, by adding the input RGW matching circuit, the complete RGW-to-sectoral GWG transition problem can be solved, e.g., using the mode-matching technique [22] or any other full-wave method. Below, we use a 2-step input RGW matching circuit, providing impedance transformation and reduction of the ridge edge capacitance [8], with the following geometric parameters (in μm): $H_{11} = 627$, $H_{12} = 379$, $L_{11} = 1203$, $L_{12} = 864$.

As an alternative to the full-wave analysis, a simple engineering approximate solution can be obtained from (2). Since the excitation RGW operates almost in the traveling-wave regime [8], provided by the 2-step matching circuit, we can consider only propagating TE_{m0} (to y) ridge modes ($B_{mn}^r = 0$). In particular, we are interested in the dual-mode RWG operation when TE_{10} and TE_{30} modes primarily contribute to the RGW field on the R_0 plane. The characteristics of these modes have been found using the integral eigenvalue formulation [23]. Fig. 2 demonstrates E-field magnitude distributions of both modes. Let us now assume the field on the RGW side of R_0 as $\mathbf{E}^r = \mathbf{e}_{10}^{\text{rTE}} + A_{30}^r \mathbf{e}_{30}^{\text{rTE}}$, with the modal coefficient A_{30}^r being the problem parameter (“+” is omitted for compactness). Then, applying the Ritz-Galerkin procedure [21] by representing the sectoral GWG field with a truncated series of M TM_{0p} modes $\mathbf{E}^s = \sum_p^M A_{0p}^s \mathbf{e}_{0p}^{\text{sTM}}$ and projecting (2) on $\mathbf{e}_{0p}^{\text{sTM}}$, we reduce the problem to the system of M linear equations with the vector of unknown coefficients $\vec{A}^s = [A_{01}^s \dots A_{0M}^s]^T$:

$$\vec{A}^s = [Q]^{-1} \vec{B}^s, \quad (3)$$

$$Q_{ij} = \int_{(R_0)} \mathbf{e}_{0i}^{\text{sTM}*} \mathbf{e}_{0j}^{\text{sTM}} ds, \quad B_i^s = \int_{(R_0)} \mathbf{e}_{0i}^{\text{sTM}*} \mathbf{E}^r ds. \quad (4)$$

The solution (3) depends on A_{30}^r , which is not known *a priori*. The full-wave analysis of the modal content, implemented in Ansys HFSS for the $(20 - 35)^\circ$ flare angle range, suggests that $A_{30}^r = (0.3 - 0.5)$. The computed relative A_{03}^s as a function of L_r obtained for $A_{30}^r = 0.4$ is demonstrated in Fig. 3 (note the TE_{30} mode cut-off at $L_r = 4.3$ mm). Here, we also show the results obtained in Ansys HFSS. As seen, the approximate method with the constant A_{30}^r fit gives a rough average estimation of the relative magnitude that converges to the full-wave solution for large L_r . The observed discrepancies are caused by A_{30}^r magnitude oscillations around the mode

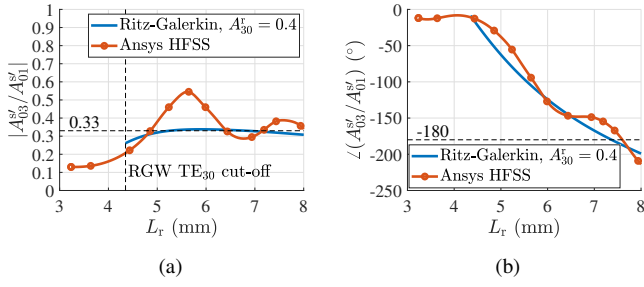


Fig. 3. Relative magnitude (a) and phase (b) curves of the sectoral GWG TM_{03} mode on the reference plane R_1 at 95 GHz computed using the full-wave simulation and the proposed approximate method ($M = 12$).

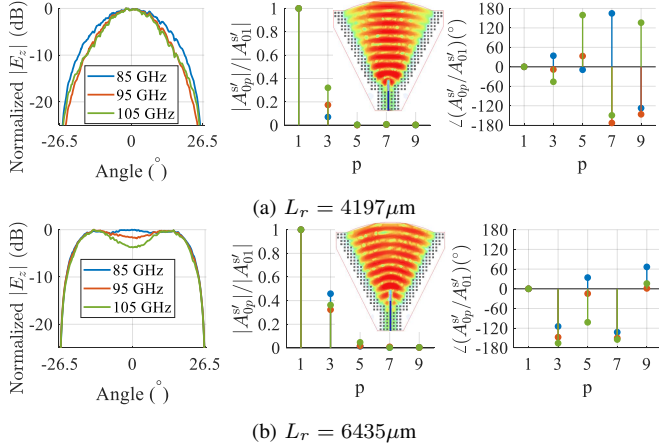


Fig. 4. Full-wave simulated E_z distributions and modal spectra on the R_1 surface at 85, 95, 105 GHz: (a) $L_r = 4197 \mu\text{m}$ and (b) $L_r = 6435 \mu\text{m}$. The insets show instantaneous E-field magnitude distributions.

cut-off region. However, the relative phase [Fig. 3(b)] is quite accurate ($\pm 20^\circ$ error) and, as found, weakly depends on A_{30}^r .

From Fig. 3, we infer that the TM_{03} sectoral GWG mode is effectively excited when $L_r > 4.5$ mm. It can be explained by approaching the mode gradual cut-off [21] defined by $\rho_p = \lambda p / (4\phi_0)$. Despite the fast growth of $|A_{03}^s|$ when $L_r > \rho_p$, some extra length is required to accumulate the desired 180° phase difference. The best field uniformity can be achieved with only TM_{03} mode since independent control of two or more higher-order modes is typically not feasible with only L_r . For the considered case, we found $L_{r, \text{opt}} = 6435 \mu\text{m}$ that provides an almost optimal A_{03}^s with a minimal ridge length. For an arbitrary value of ϕ_0 the optimal length was estimated as $L_{r, \text{opt}} \approx \lambda / \phi_0$. Fig. 4 demonstrates computed E_z distributions and modal spectra on the R_1 surface for a reduced and optimal L_r that supports our finding on the optimal ridge length. In conclusion, the proposed simple analysis method can be effectively employed to find a first-order approximation of $L_{r, \text{opt}}$, which can be further refined by full-wave simulations.

B. Sectoral GWG-to-Rectangular GGW Transition

To further enhance the field uniformity, the sectoral GWG is transitioned to the rectangular GGW, as Fig. 5 shows. The total E-field of the rectangular GGW can be approximated by a superposition of rectangular WG TE_{m0} modal fields propagating in the positive y -direction [21]:

$$\mathbf{E}^g(x, y) = \mathbf{z}^0 \sum_m^K A_{m0}^g \cos\left(\frac{m\pi}{D}x\right) e^{-jk_{ym0}(y-F)}, \quad (5)$$

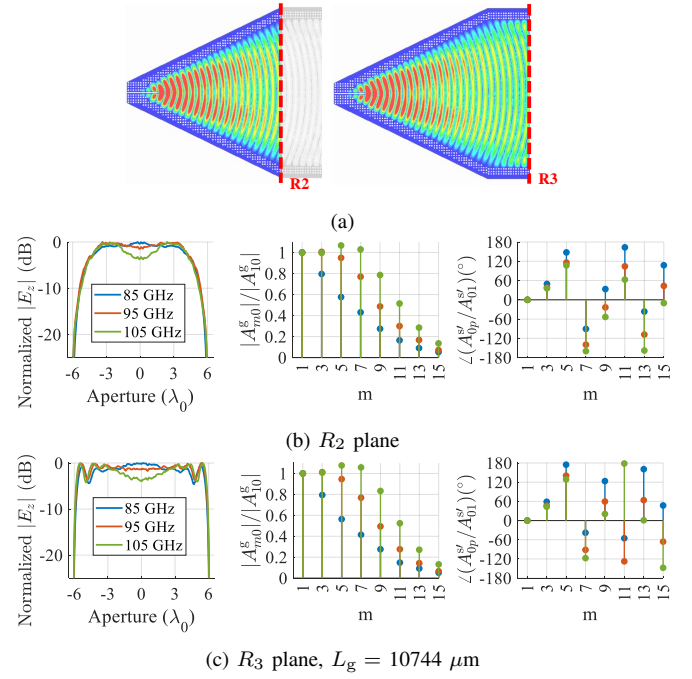


Fig. 5. Instantaneous E-field magnitude distributions (a) and modal spectra on the (b) R_2 and (c) R_3 surface of the GWG QO feed ($L_r = 6435 \mu\text{m}$).

where A_{m0}^g are modal complex coefficients, $k_{ym0} = \sqrt{k^2 - \left(\frac{m\pi}{D}\right)^2}$ are the propagation constants of the TE_{m0} (to y) modes, and $D = N_x d_x$; m is odd; K is the highest propagation mode index. Fig. 5 demonstrates a full-wave simulated E_z when the GGW is terminated with the ABC on R_3 . As seen, the transition between two overmoded WGs represents a “soft” discontinuity: the incident sectoral GWG field excites a multi-modal rectangular GGW spectrum on R_2 without generating reflections. This rich spectrum can be further used to improve the field uniformity in the edge QO areas. To achieve this, we utilize a uniform GGW section of length L_g . Neglecting a propagation loss, the only spectrum change between R_2 and R_3 involves a relative mode phase accumulation $\Delta\varphi_m = (k_{ym0} - k_{y10})L_g$. The length L_g is then optimized numerically to achieve the best taper efficiency. We may note that the presented approach shares a similar idea with the Potter horn antenna [24]. Fig. 5(c) demonstrates the spectrum on the R_3 plane for the optimal $L_g = 10744 \mu\text{m}$. We observe that L_g primarily affects the higher-order mode phases ($m > 5$). This helps to improve the taper efficiency [25] from 88% (on R_2) to 96% (on R_3). Fig. 6(a) presents a final parametric study on the full QO geometry, showing the taper efficiency versus frequency for various L_r and the optimal L_g . As expected, a highest taper efficiency of $\geq 96\%$ is achieved for $L_{r, \text{opt}} = 6435 \mu\text{m}$ over the 21% BW.

Finally, the rectangular GGW was loaded with the 20-element RGW probe array [8]. The simulated S -parameters of the complete feed are shown in Fig. 6(b) and demonstrate ≤ -17 dB reflection, ≤ 5.4 dB amplitude imbalance (primarily due to the edge element suppression), and ≤ 0.4 dB insertion loss. The taper efficiency of the feed $\geq 97\%$. Note that for this simulation the whole structure was made of aluminum with the $0.5 \mu\text{m}$ Grosse surface roughness model.

TABLE I
PERFORMANCE COMPARISON OF THE REPORTED QO H-PLANE FEEDING NETWORKS.

	Technology	Quasi-optical geometry	f_0 (GHz); BW	Taper efficiency; amplitude taper (dB)	Insertion loss (dB)
[20]	Aluminium RGW	Sect. RGW (single-mode) + parabolic reflector	15; 41%	$\geq 90\%$; ≥ 6	N/A
[16]	Air-filled SIW	Sect. WG (single-mode) + 1×4 array	43; 21%	N/A; ≤ 1	≤ 1.5 ^{est}
[11]	Aluminium GWG	PPW [†] + parabolic reflector + 1×16 array	93; 38%	N/A; ≥ 15 ^{est}	≤ 1.3
[19]	Micromachined WG	PPW pillbox + parabolic reflector + 1×39 array	260; 23%	87% ^{est} ; 15	≤ 1.6 ^{ant}
This work	Aluminium GWG	Sect. GWG (multi-mode) + rect. GGW + 1×20 array	95; 21%	$\geq 97\%$; ≤ 5.1	≤ 0.4

^{est} Estimated from field plots; [†] Parallel-plate WG; ^{ant} full antenna.

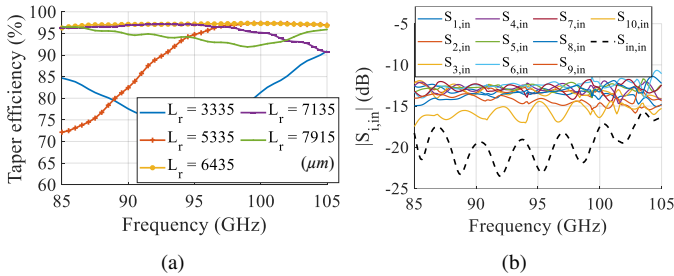


Fig. 6. (a) Taper efficiency of the QO feed (R_3 plane); (b) S -parameters of the full QO feed with the 1×20 array of output RGW probes (R_4 plane).

IV. MEASUREMENT RESULTS AND DISCUSSION

Since the physical spacing between the output RGWs d_x is much smaller than the standard WR-10 WG interface, we connected a linear 1×20 array antenna [9] to the QO feed outputs to validate the proposed approach by measuring the antenna far field (Fig. 1). At this stage, PS circuits were not incorporated. The whole structure, presented in Fig. 7, was CNC-milled from aluminum. The array was interfaced with the WR-10 WG through an input orthogonal transition [9] and measured at Chalmers THz antenna test chamber. Fig. 8 demonstrates a great agreement between simulated and measured results. In the targeted band, the measured reflection coefficient is ≤ -12 dB [Fig. 8(a)]. The far-field performance is detailed in Figs. 8(b),8(c),8(d) for the broadside realized gain, H-plane amplitude and phase radiation patterns, respectively. The observed gain fluctuations across frequencies are attributed to a non-compensated QO feed phase front. Some minor pattern discrepancies can be seen below -20 dB relative amplitude pattern level. The latter is believed to be caused by the measurement chamber's accuracy. Given the prior validation of linear array radiation patterns [9], these results implicitly evidence that the expected output amplitude-phase distribution was successfully realized by the QO feed.

Table I compares the presented design with the published H-plane QO feeds, employing various QO geometries, and shows its superior performance in terms of a state-of-the-art combination of high taper efficiency and low insertion loss.

V. CONCLUSIONS

The proposed QO feed achieves a nearly uniform amplitude of the array elements illumination field owing to the optimal ridge excitation of the multi-modal H-plane sectoral GGW and the proper mode phasing of the output GGW. To alleviate the design complexity associated with full-wave numerical simulations, one can employ an approximate mode-matching solution to identify the desired modal content and predict an approximate optimal ridge length. The QO feed, applied

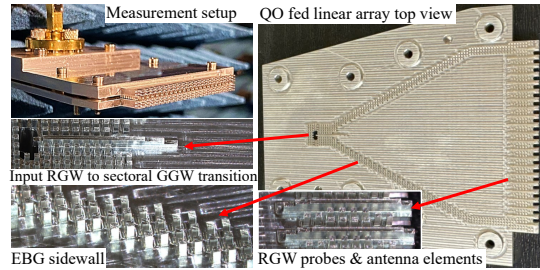


Fig. 7. The fabricated array at Chalmers THz antenna test chamber and photographs of the main design parts (top plate removed).

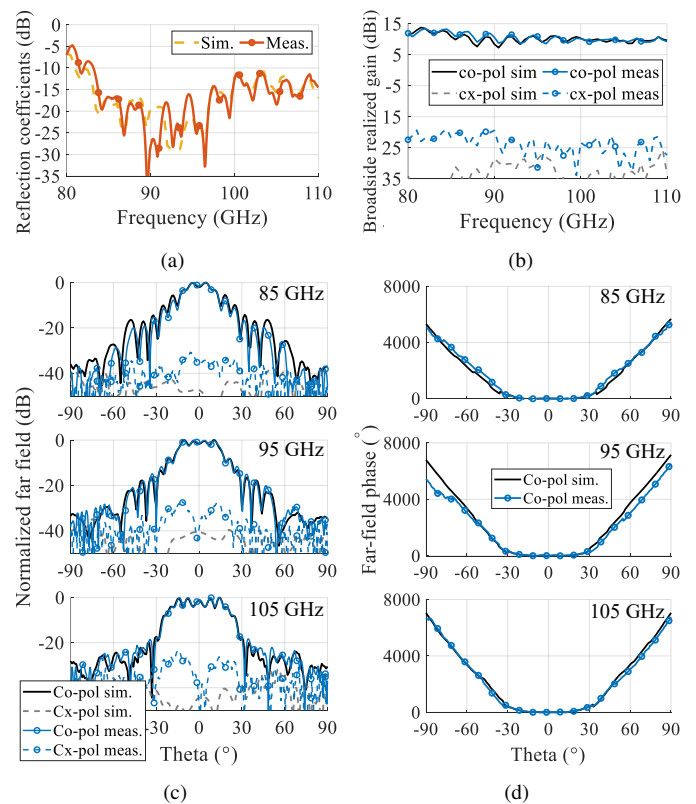


Fig. 8. Simulated and measured performance of the linear array with the QO feed: (a) reflection coefficient and (b) broadside realized gain; (c) normalized amplitude and (d) co-polarized phase H-plane patterns at 85, 95, 105 GHz.

to the 20-element array antenna, demonstrates outstanding performance with 97% taper efficiency and less than 0.4 dB insertion loss over the 21% relative bandwidth (85–105 GHz). A potential design improvement involves reducing the overall longitudinal dimension, e.g., through folding.

REFERENCES

- [1] "European vision for the 6G network ecosystem," White Paper, The 5G Infrastructure Association, Jun. 2021.
- [2] X. Gu, D. Liu, and B. Sadhu, "Packaging and antenna integration for silicon-based millimeter-wave phased arrays: 5G and beyond," *IEEE Journal of Microwaves*, vol. 1, no. 1, pp. 123–134, 2021.
- [3] T. S. Rappaport, Y. Xing, O. Kanhere, S. Ju, A. Madanayake, S. Mandal, A. Alkhatieb, and G. C. Trichopoulos, "Wireless communications and applications above 100 GHz: Opportunities and challenges for 6G and beyond," *IEEE Access*, no. 7, pp. 78 729–78 757, 2019.
- [4] A. R. Vilenskiy, E. Galesloot, Y. Zhang, A. B. Smolders, and M. V. Ivashina, "Quasi-optical beamforming network for millimeter-wave electronically scanned array antennas with 1-bit phase resolution," in *2021 15th European Conference on Antennas and Propagation (EuCAP)*. IEEE, 2021, pp. 1–5.
- [5] A. R. Vilenskiy, M. N. Makurin, C. Lee, and M. V. Ivashina, "Reconfigurable transmitarray with near-field coupling to gap waveguide array antenna for efficient 2D beam steering," *IEEE Trans. Antennas Propag.*, vol. 68, no. 12, pp. 7854–7865, Dec. 2020.
- [6] A. Clemente, F. Diaby, L. D. Palma, L. Dussopt, and R. Sauleau, "Experimental validation of a 2-bit reconfigurable unit-cell for transmitarrays at Ka-band," *IEEE Access*, vol. 8, pp. 114 991–114 997, 2020.
- [7] X. Pan, S. Wang, G. Li, S. Xu, and F. Yang, "On-chip reconfigurable reflectarray for 2-D beam-steering at w-band," in *2018 IEEE MTT-S International Wireless Symposium (IWS)*. IEEE, 2018, pp. 1–4.
- [8] A. R. Vilenskiy, Y. Zhang, E. Galesloot, A. B. Smolders, and M. V. Ivashina, "Millimeter-wave quasi-optical feeds for linear array antennas in gap waveguide technology," in *2022 16th European Conference on Antennas and Propagation (EuCAP)*. IEEE, 2022, pp. 1–5.
- [9] Y. Zhang, A. R. Vilenskiy, and M. V. Ivashina, "Wideband open-ended ridge gap waveguide antenna elements for 1-D and 2-D wide-angle scanning phased arrays at 100 ghz," *IEEE Antennas and Wireless Propagation Letters*, vol. 21, no. 5, pp. 883–887, 2022.
- [10] A. R. Vilenskiy and Y. Zhang, "A compact and wideband MMIC to ridge gap waveguide contactless transition for phased array antenna front-ends," *IEEE Antennas and Wireless Propagation Letters*, pp. 1–5, 2023, early access.
- [11] R. Maaskant, W. A. Shah, A. U. Zaman, M. Ivashina, and P.-S. Kildal, "Spatial power combining and splitting in gap waveguide technology," *IEEE Microwave and Wireless Components Letters*, vol. 26, no. 7, pp. 472–474, 2016.
- [12] A. Biedma-Pérez, P. Padilla, C. Segura-Gómez, and A. Palomares-Caballero, "Holey siw horn antenna based on an H-plane lenswise wavefront collimation," *IEEE Transactions on Antennas and Propagation*, vol. 71, no. 1, pp. 1023–1028, 2022.
- [13] W. Yuan, J. F. Chen, C. Zhang, W. X. Tang, L. Wang, Q. Cheng, and T. J. Cui, "Glide-symmetric lens antenna in gap waveguide technology," *IEEE Transactions on Antennas and Propagation*, vol. 68, no. 4, pp. 2612–2620, 2019.
- [14] J.-Y. Deng, R.-Q. Luo, W. Lin, Y. Zhang, D. Sun, X.-M. Zhang, and L.-X. Guo, "Horn antenna with miniaturized size and increased gain by loading slow wave periodic metal blocks," *IEEE Transactions on Antennas and Propagation*, vol. 69, no. 4, pp. 2365–2369, 2020.
- [15] J.-Y. Deng, R.-Q. Luo, W. Lin, Y. Zhang, Z. Chen, and L.-X. Guo, "Longitudinally miniaturized h-plane horn antenna with 30 dB sidelobes realized by simple blocks redistributing the aperture field," *IEEE Transactions on Antennas and Propagation*, vol. 70, no. 8, pp. 7187–7192, 2022.
- [16] J. Wang, F. Wu, Z. H. Jiang, Y. Li, and D. Jiang, "A millimeter-wave substrate integrated waveguide h-plane horn antenna with enhanced gain and efficiency," *IEEE Antennas and Wireless Propagation Letters*, vol. 21, no. 4, pp. 769–773, 2022.
- [17] M. Chen, F. Mesa, and O. Quevedo-Teruel, "Geodesic H-plane horn antennas," *IEEE Transactions on Antennas and Propagation*, 2023.
- [18] J. G. Nicholls and S. V. Hum, "Full-space electronic beam-steering transmitarray with integrated leaky-wave feed," *IEEE Transactions on Antennas and Propagation*, vol. 64, no. 8, pp. 3410–3422, 2016.
- [19] A. Gomez-Torrent, M. Garcia-Vigueras, L. Le Coq, A. Mahmoud, M. Ettore, R. Sauleau, and J. Oberhammer, "A low-profile and high-gain frequency beam steering subterahertz antenna enabled by silicon micromachining," *IEEE Trans. Antennas Propag.*, vol. 68, no. 2, pp. 672–682, 2020.
- [20] E. Sabbaghi, S. A. Razavi, and M. H. Ostovarzadeh, "Wide band ridge gap waveguide (RGW) fan beam antenna with low side lobes based on parabolic reflector principle," *IET Microwaves, Antennas & Propagation*, vol. 14, pp. 343–347, 2020.
- [21] R. F. Harrington, *Time harmonic electromagnetic fields*. Wiley-IEEE Press, 2001.
- [22] R. Mittra and S. W. Lee, *Analytical techniques in the theory of guided waves*. Macmillan, New York, 1971.
- [23] J. Montgomery, "On the complete eigenvalue solution of ridged waveguide," *IEEE Transactions on Microwave Theory and Techniques*, vol. 19, no. 6, pp. 547–555, 1971.
- [24] P. D. Potter, "A new horn antenna with suppressed sidelobes and equal beamwidths," *Microwave Journal*, vol. 19, no. 6, p. 71–78, 1963.
- [25] P.-S. Kildal, *Foundations of antenna engineering: a unified approach for line-of-sight and multipath*. Artech House, 2015.